

Dissipative cooling towards phantom Bethe states in boundary driven XXZ spin chain

Vladislav Popkov^{1,2} and Mario Salerno³

¹*Faculty of Mathematics and Physics, University of Ljubljana, Jadranska 19, SI-1000 Ljubljana, Slovenia*

²*Bergisches Universität Wuppertal, Gauss Str. 20, D-42097 Wuppertal, Germany*

³*Dipartimento di Fisica “E.R. Caianiello”, and INFN - Gruppo Collegato di Salerno, Università di Salerno, Via Giovanni Paolo II, 84084 Fisciano (SA), Italy*

(Dated: September 27, 2022)

A dissipative method that allows to access family of phantom Bethe-states (PBS) of boundary driven XXZ spin chains, is introduced. The method consists in coupling the ends of the open spin chain to suitable dissipative magnetic baths to force the edge spins to satisfy specific boundary conditions necessary for the PBS existence. Cumulative monotonous depopulation of the non-chiral components of the density matrix with growing dissipation amplitude is analogous to the depopulation of high-energy states in response to thermal cooling. Compared to generic states, PBS have strong chirality, nontrivial topology and carry high spin currents.

Introduction. Dissipation needs not to be always destructive for quantum protocols but it can represent a resource for manipulating quantum systems. Dissipation alone [1] or in combination with coherent dynamics [2–10], indeed, can be used to create quantum non-equilibrium stationary states (NESS) which are attractors of the dynamics and therefore are stable even in the presence of noise.

Most protocols, however, require a tailored set of operations used in pumping cycles to target each specific state [5, 11]. If the protocols are implemented by stationary control fields, they usually require sophisticated dissipations that make the NESS targeting more complicated [12]. This is due to the fact that the targeted NESS must be an eigenstate of the coherent part of the dynamics and a dark state for all jump operators in the dissipator [13, 14].

Here we demonstrate how to generate a remarkable family of NESS containing an arbitrary number of qubits, employing simple boundary-localized dissipation, and manipulating just one parameter. These are the phantom Bethe states (PBS), i.e. eigenstates of integrable XXZ spin chains on special parameter manifolds [15–17], possessing unusual chiral and topological features.

The phenomenon is based on a subtle mechanism that makes (within the quantum Zeno limit [18–21]), a highly selective ‘phantom’ invariant subspace the basin of attraction for the density matrix. Consequently, the NESS responds in a singular resonant way to an increase of the dissipation strength in the vicinity of “phantom” manifolds, restricting the density matrix to states with chirality of the same sign and thus rendering the NESS chiral. The resonances become sharper as the dissipation strength is increased and their number grows with the number of spins involved.

Dynamically, the “freezing out” of the non-chiral components of the density matrix with growing dissipation amplitude is analogous to the depopulation of high-energy states in response to thermal cooling.

The “dissipative cooling” method consists in coupling

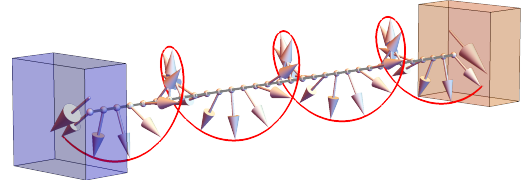


FIG. 1. Model setup. An open XXZ spin chain is edge-coupled to dissipative fully polarizing baths (blue and pink boxes). When baths’s polarizations (big arrows inside boxes) match Eq. (8), phantom Bethe states carrying large spin currents come into existence. The figure shows a pure spin-helix state corresponding to case $M_+ = 0$ in Eq. (8).

the ends of the open chain to dissipative baths of polarization constraining the first and the last spin to relax to predefined pure qubit states that satisfy boundary conditions necessary for the PBS existence. We show that by changing the control parameter, i.e. the misfit azimuthal angle of the dissipatively-targeted boundary polarizations, it is possible to thread “phantom” manifolds, passing from one chiral NESS to another one with different topology (see Figs. 2). To the best of our knowledge, a quantum protocol that allows to target the whole PBS family is presently lacking.

The simplest states belonging to the phantom family are the spin-helix states (SHS) (see top panel of Fig. 4 for an example). Recently, SHS were created and used as a sensitive tool to measure the anisotropy in experiments on XXZ chains implemented via ultracold atoms [22, 23]. While in [22, 23], the lifetime of the SHS is restricted by finite size effects, the stability of dissipatively created SHS (and other PBS) is guaranteed as long as the boundary dissipation strength is kept sufficiently strong.

Note that while SHS are pure states, all other PBS are mixed states corresponding, in terms of the mean variation of the magnetization along the chain, to helices with a variable radius (see middle panel of Fig. 4 for an example). Quite interestingly, we find that in comparison to generic pure and mixed states of the open XXZ

chain, the PBS have strong chirality and carry relatively high spin currents (see Fig.3), a feature that can be of potential interest for future applications.

Model setting and near Zeno limit relaxation. Our dissipative setup is schematically depicted in Fig. 1. An XXZ Heisenberg spin $\frac{1}{2}$ chain of $N+2$ sites, numbered as $0, 1, \dots, N+1$, is coupled to Lindbladian baths of polarizations at the ends ([18, 24], see details in [25]). We assume dissipative targeting of generic pure qubit states $\rho_{L,R} = (I + \vec{n}_{L,R} \cdot \vec{\sigma})/2$ at sites 0 and $N+1$, where \vec{n}_L, \vec{n}_R are unit vectors of polarization. The strength of the dissipation Γ is measured by the inverse time needed for edge spins to relax, e.g. $\rho_{L/R}(t) = \frac{I}{2} + \frac{1}{2}\vec{\sigma}_1\vec{n}_{L/R} + O(e^{-\Gamma t})$, if the coherent part (XXZ spin chain Hamiltonian) is neglected. If $\vec{n}_L \neq \vec{n}_R$, a nonequilibrium gradient is created and a spin current j^z can flow, typically obeying the Fourier law $j^z = O(1/N)$.

In (8) we fix a resonance condition under which steady currents can be increased up to maximally possible values, $j^z = O(1)$. Using the criterion of [26] one finds that the NESS is always unique.

It was shown in [27] that close to quantum Zeno limit $\Gamma \rightarrow \infty$ the relaxation to NESS undergoes a three-stage process, each stage occurring at different timescale. On the shortest timescale: $t \leq O(1/\Gamma)$, the boundary spins relax towards their targeted states. From this point on, the density matrix is approximately given by $\rho = \rho_L \otimes R(t) \otimes \rho_R$, where $R(t) = \text{tr}_{L,R}\rho(t)$ describes the time evolution of the internal part of the system, which becomes approximately coherent again [2] and is governed by the dissipation projected Hamiltonian h_D given by [27]

$$h_D = \sum_{n=1}^{N-1} \vec{\sigma}_n \cdot \hat{J}\vec{\sigma}_{n+1} + \hat{J}\vec{n}_L \cdot \vec{\sigma}_1 + \hat{J}\vec{n}_R \cdot \vec{\sigma}_N, \quad (1)$$

with $\hat{J} = \text{diag}(1, 1, \Delta)$. Note that the dissipation-projected Hamiltonian (1) depends on polarizations of the baths through its boundary fields.

On the intermediate timescale: $O(1/\Gamma) \ll t \leq O(1)$, the reduced density matrix $R(t)$ acquires the approximate form

$$R(t) = \sum_{\alpha} P_{\alpha}(\tau) |\alpha\rangle\langle\alpha| + O\left(\frac{1}{\Gamma}\right), \quad (2)$$

where $\tau = \frac{t}{\Gamma}$ and $|\alpha\rangle$ are h_D eigenstates, with positive coefficients P_{α} significantly changing on long time scales $\tau = O(1)$. Finally, on the long time scale $O(1) \ll t \leq O(\Gamma)$ the coefficients $P_{\alpha}(\tau) \rightarrow P_{\alpha}(\infty) \equiv P_{\alpha}$ relax to their stationary NESS values, by following an effective Markov process

$$\frac{\partial P_{\alpha}(\tau)}{\partial \tau} = \sum_{\beta \neq \alpha} w_{\beta\alpha} P_{\beta}(\tau) - \sum_{\beta \neq \alpha} w_{\alpha\beta} P_{\alpha}(\tau) \quad (3)$$

with rates $w_{\alpha\beta} \equiv w_{\alpha \rightarrow \beta}$ given by [27]

$$w_{\alpha\beta} = |\langle\beta|g_L|\alpha\rangle|^2 + |\langle\beta|g_R|\alpha\rangle|^2, \quad (4)$$

where g_L, g_R are operators acting on the first and the last spin respectively, given by

$$g_L = g(\vec{n}_L) \otimes I^{\otimes N-1}, \quad g_R = I^{\otimes N-1} \otimes g(\vec{n}_R), \quad (5)$$

$$g(\vec{n}(\theta, \varphi)) = \hat{J} \left(\vec{n}\left(\frac{\pi}{2} - \theta, \varphi + \pi\right) - i\vec{n}\left(\frac{\pi}{2}, \varphi + \frac{\pi}{2}\right) \right) \cdot \vec{\sigma}, \quad (6)$$

where θ, φ are spherical coordinates of a unit vector. The final state, the NESS, in the Zeno limit has the form

$$\rho_{NESS}^{Zeno} = \rho_L \otimes \left(\sum_{\alpha} P_{\alpha} |\alpha\rangle\langle\alpha| \right) \otimes \rho_R, \quad (7)$$

where P_{α} is time-independent solution of (3), and $|\alpha\rangle$ are eigenstates of h_D (1).

Phantom Bethe states. Phantom Bethe states are eigenstates of the Hamiltonian (1) that have exceptional chirality and correspond to special manifolds of the boundary fields in (1) $\hat{J}\vec{n}_L(\theta_L, \varphi_L), \hat{J}\vec{n}_R(\theta_R, \varphi_R)$, with θ, φ given by [15, 16]

$$\theta_L = \theta_R, \quad \varphi_R - \varphi_L = (N+1 - 2M_+) \gamma, \quad (8)$$

where $M_+ = 0, 1, \dots, N+1$ [28] and γ parametrizing the XXZ model anisotropy Δ

$$\Delta = \cos \gamma. \quad (9)$$

The substitution $M_+ \rightarrow M_- \equiv N+1 - M_+$ in (8) leads to the physical setup with the opposite boundary gradient, $\varphi_R - \varphi_L \rightarrow -(\varphi_R - \varphi_L)$, and consequently flips the steady current $j^z \rightarrow -j^z$. The respective NESSs are related via the left-right reflection $\varphi_L \leftrightarrow \varphi_R$ and subsequent rotation in XY -plane, see [25]. Using this property we restrict the M_+ range to the $M_+ = 0, 1, \dots, \lfloor \frac{N+1}{2} \rfloor$.

For fixed $M \equiv M_+$ in this range all eigenstates $|\alpha\rangle$ of h_D (1) which determine Zeno NESS (7) split into two chiral families, $\{|\alpha_+\rangle\}, \{|\alpha_-\rangle\}$ characterized by the so-called phantom Bethe roots [15]. All eigenstates from each family share common chiral properties [16]. Introducing the function $b(n, m) = \sum_{k=n}^m \binom{N}{k}$, the number of eigenstates d_+, d_- in $\{|\alpha_+\rangle\}, \{|\alpha_-\rangle\}$ is given by $d_{\pm} = b(0, M_{\pm})$. In addition, in our case (8) a smaller invariant subfamily $\{|\alpha_+^{(1)}\rangle\} \in \{|\alpha_+\rangle\}$ exists [25], yielding further splitting $\{|\alpha_+\rangle\} = \{|\alpha_+^{(1)}\rangle\} \oplus \{|\alpha_+^{(2)}\rangle\}$ where $d_+^{(1)} = b(M-1, M) = \binom{N+1}{M}$, $d_+^{(2)} = b(0, M-2)$.

According to the above, the reduced density matrix R in (2) on ‘‘phantom’’ manifolds (8) splits as

$$R \approx \sum_{\kappa=1}^2 \sum_{\alpha_+^{(\kappa)}=1}^{d_+^{(\kappa)}} P_{\alpha_+^{(\kappa)}}(\tau) |\alpha_+^{(\kappa)}\rangle\langle\alpha_+^{(\kappa)}| + \sum_{\alpha_-=1}^{d_-} P_{\alpha_-}(\tau) |\alpha_-\rangle\langle\alpha_-|. \quad (10)$$

The sum (10) contains projectors on states with opposite chiralities and is generically approximately neutral. The time evolution obeys the effective Markov process (3) i.e. depends on rates $w_{\beta\delta}$ exclusively. Analyzing the rates [25] we find a remarkable property: all the rates

$$w_{\alpha_+^{(1)} \rightarrow \alpha_-} = w_{\alpha_+^{(1)} \rightarrow \alpha_+^{(2)}} = 0 \quad (11)$$

vanish, while generic $w_{\beta \rightarrow \alpha_+^{(1)}}$ remain finite. Thus, the subfamily $\{|\alpha_+^{(1)}\rangle\}$ becomes an adsorbing basin of the Markov process (3) [29] resulting in depopulation of all other states with time, and leading to the NESS of the form

$$\rho_{NESS}^{Phantom}(M) = \rho_L \otimes \left(\sum_{\alpha_+^{(1)}=1}^{\binom{N+1}{M}} P_{\alpha_+^{(1)}} |\alpha_+^{(1)}\rangle \langle \alpha_+^{(1)}| \right) \otimes \rho_R. \quad (12)$$

All eigenstates $|\alpha_+^{(1)}\rangle$ in (12) are phantom Bethe eigenstates [15] of the same chirality and the chirality gets more pronounced for small M . For $M = 0$, the sum in (12) contains just one term, a projector on the spin-helix state (SHS) (13)

$$\Psi_{SHS}(\gamma) = \bigotimes_{k=1}^N \begin{pmatrix} \cos \frac{\theta_L}{2} \\ \sin \frac{\theta_L}{2} e^{ik\gamma + i\varphi_L} \end{pmatrix}, \quad (13)$$

visualized in Fig. 1, characterized by a large current of magnetization

$$j_{SHS} = \langle 2(\sigma_n^x \sigma_{n+1}^y - \sigma_n^y \sigma_{n+1}^x) \rangle_{SHS} = 2 \sin^2 \theta_L \sin \gamma. \quad (14)$$

A possibility to target spin-helix state (13) dissipatively was also noted in previous studies [14, 30, 31].

For $M > 0$ the ideal helix (13) gets blurred but the NESS (12) remains chiral. For $M = 1$ the current of magnetization $\langle \alpha_+ | \hat{j}^z | \alpha_+ \rangle$ averaged over states $|\alpha_+ \rangle$ is of the order $\langle j^z(M) \rangle \approx j_{SHS}(1 - 2/N)$, while for arbitrary $M < N/2$, estimates yield $\langle j^z(M) \rangle \approx j_{SHS}(1 - 2M/N)$ [16].

From the above result we predict the existence of chiral Zeno NESS with unusually high magnetization current at phantom Bethe manifolds (8).

Numerical results. To check our predictions we study NESS magnetization current for fixed anisotropy Δ and varying boundary gradient, for systems of size $4 \leq N \leq 30$. We use exact numerical diagonalization for small chains [32] and Matrix product ansatz for NESS in the Zeno limit [33, 34] for large chains. Already for $N = 5$ we find all j^z peak positions at predicted points (8) and their vicinity, see Figs. 2. Namely, all points (8) with $M_{\pm} = 0, 1, 2$ correspond to peaks of various amplitudes ($j^z = 0$ for $M_+ = (N + 1)/2 = 3$, since it corresponds to

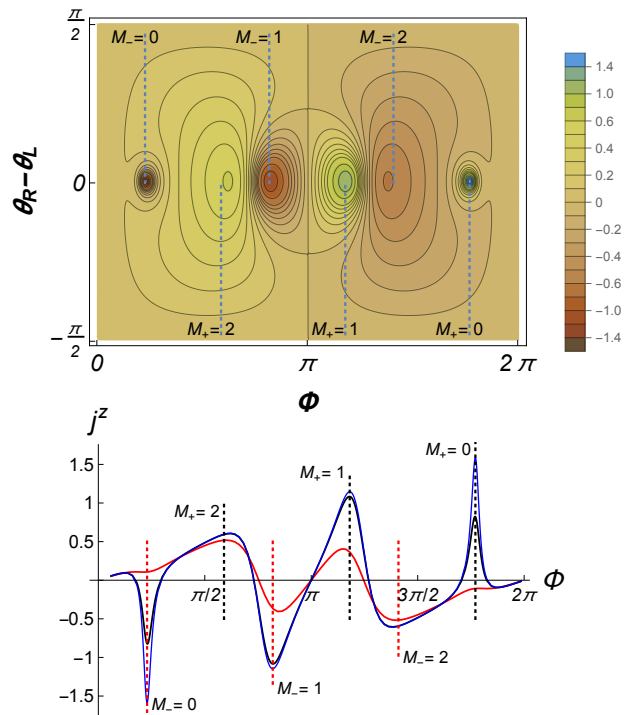


FIG. 2. **Top Panel:** Steady magnetization current j^z versus boundary misfits of azimuthal angle $\Phi = \varphi_R - \varphi_L$ and polar angle $\theta_R - \theta_L$, in Zeno limit, for $N = 5, \Delta = 0.6, \theta_L = \pi/2$. The targeted spin polarizations are $\vec{n}_L = (1, 0, 0), \vec{n}_R = (\sin \theta_R \cos \Phi, \sin \theta_R \sin \Phi, \cos \theta_R)$. **Bottom Panel:** cut of the j^z surface at $\theta_R - \theta_L = 0$, for different dissipation strengths $\Gamma = 20, 100, 1000$ (more spiky functions correspond to increasing Γ). Vertical black and red dotted lines indicate the misfit angles $\Phi = \pm(N + 1 - 2M)\gamma$.

zero misfit angle $\Phi = \pm(N + 1 - 2M_+)\gamma = 0$ and hence to absence of the boundary gradient $\vec{n}_L = \vec{n}_R$).

For larger chains (Fig. 3) the agreement and the phenomenon becomes striking: most j^z peaks appear as sharp resonances centered at phantom Bethe states manifolds (8), on top of a background with $j^z = O(1/N)$. Notice that the empty black and red circles in (Fig. 3) show the dependence of the j^z peaks on M (top horizontal axis).

The role of the parameter M determining the NESS rank in (12) via $r(M) = \binom{N+1}{M}$ deserves special discussion. The highest and sharpest of all j^z peaks always corresponds to $M_{\pm} = 0$, see Figs. 2, 3, i.e. pure Zeno NESS, with magnetization winding in a perfect helix around the z axis, see (13) and Fig. 4. For $M > 0$, perfect chirality is lost: the basis of “phantom” manifold for $M = 1$ consists of 2 disjointed helix pieces separated by a kink at some position n ; phantom Bethe states are linear combinations of basis states for all possible kink positions [16]. Resulting NESS magnetization profile is a distorted helix with variable radius, see mid-panel of Fig. 4. Basis states for arbitrary M contain M kinks [16], introducing more helix imperfections. For large M NESS becomes a

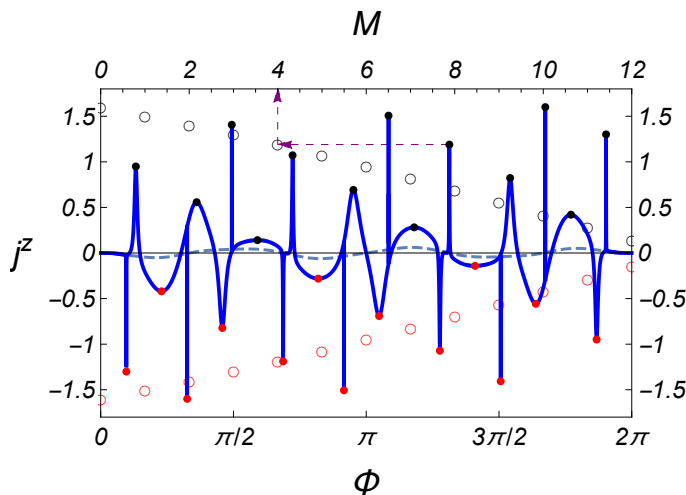


FIG. 3. Steady magnetization current j^z (blue curve) versus XY -plane misfit angle $\Phi = \varphi_R - \varphi_L$ (bottom horizontal-axis) in the Zeno limit $\Gamma \rightarrow \infty$, computed using method in [33, 34]. Parameters are: $N = 25$, $\Delta = 0.6$, $\theta = \pi/2$. Φ coordinates of black/red dots correspond to angles $\Phi_c(M) = \varphi_R - \varphi_L$ with $M = 0, 1, \dots, N+1$ in (8). The dashed blue line shows j_z versus Φ for a chain with an additional boundary misfit $\pi/6$ in the polar angle: $\vec{n}_L = (1, 0, 0)$, $\vec{n}_R = (\frac{\sqrt{3}}{2} \cos \Phi, \frac{\sqrt{3}}{2} \sin \Phi, \frac{1}{2})$. The empty black and red circles referring to the top horizontal-axis permit to identify the values of M associated to each j^z peak, as indicated by the purple dashed lines with arrows (find the corresponding open circle of equal amplitude and read the M value on the top-horizontal axis).

mixture of exponentially large number of states. E.g. the peak with $M = 8$ in Fig. 3 has $\binom{26}{8} > 1.5 \cdot 10^6$ contributing states, about 5% of full Hilbert space containing 2^{25} states. Nevertheless, due to the similar chiral properties of all contributing components, the respective NESS is chiral.

In Fig are shown typical magnetization profiles of PBS of the XXZ chain with $N = 25$. We see that for each M there is a specific variation of the helix radius (curves in the bottom panel) for the corresponding PBS profile. Notice that as M increases the curves accumulate toward a limiting curve which is well above the curve corresponding to a generic NESS out of the phantom manifold (bottom red line with dots). Thus, quite interestingly, the magnetization profiles for all “phantom” manifolds $0 < M \leq N/2$ are qualitatively different from that of typical (non-chiral) NESS, a fact that well correlates with the large j^z current carried by PBS with respect to typical NESS.

In Fig. 4 we shown typical PBS profiles of the XXZ chain with $N = 25$, for different M values. We see that for each M there is a specific variation of the helix radius (curves in the bottom panel) for the corresponding PBS. Notice that as M increases the PBS curves accumulate toward a limiting curve which is well above the curve corresponding to a generic NESS out of the phan-

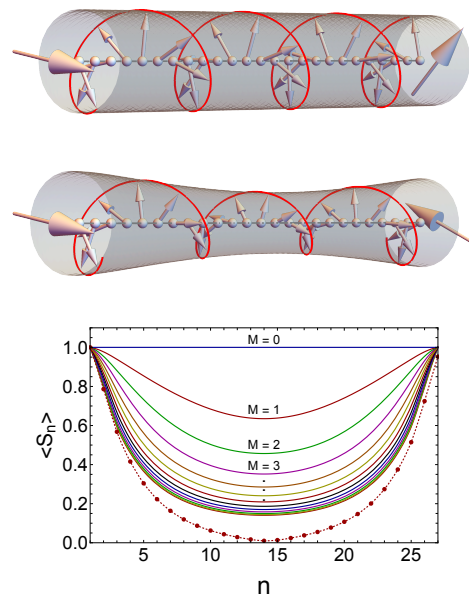


FIG. 4. **Top and middle panels.** PBS of the XXZ open chain with $N = 25$ and for cases $M = 0$ (top panel) and $M = 1$ (middle panel) in Eq.(8). The z -axis is directed along the chain while the left big arrow points in the positive x -direction. **Bottom panel:** Variation of the averaged spin (helix radius) along the chain for $M = 0, 1, \dots, 12$ (curves from top to bottom, respectively). The dotted curve at the bottom, depicted for comparison, refers to a generic NESS out of the phantom manifold. All parameters are fixed as in Fig. 3.

tom manifold (bottom line with dots). Thus, quite interestingly, the magnetization profile for all “phantom” manifolds $0 < M \leq N/2$ is qualitatively different from that of typical (non-chiral) NESS. This fact also well correlates with the large j^z current observed for PBS with respect to typical NESS.

It is also worth to note that, due to larger number of contributing states, peaks with larger M are less sharp and have smaller amplitude, but, on the other side, the NESS gets more stable with respect to perturbations (boundary misfits, lowering dissipation, etc.). This effect can be seen by comparing the behavior of peaks at increasing $\theta_R - \theta_L$ misfit (upper panel of Fig. 2) and for different Γ values (the bottom panel).

In particular, as Γ decreases, the near Zeno limit description of an effectively coherent evolution (2) becomes invalid, and the peaks gradually smear out, the sharper peaks first.

In contrast, for parameters chosen away from “phantom” manifolds, variations of Γ do not lead to any drastic effects (data not shown), especially for large enough N . The reason is, beyond certain characteristic value $\Gamma > \Gamma_{ch}(N) = O(1/N)$, effective quantum Zeno regime sets in.

Conclusion. We demonstrated that the spikes of the steady magnetization current in open XXZ spin chains

with dissipatively created boundary gradient are due to the existence of special manifolds (8) where phantom Bethe roots solutions of the Bethe Ansatz equations exist. The mechanism by which the PBS can be physically accessed was identified to be strong dissipation, which drives the system towards a chiral invariant subspace. The gradual depopulation of the non-chiral states resembles the depopulation of highly energetic states in a quantum system coupled to a cold thermal bath. The amplitude of dissipation plays the role of inverse temperature and a chiral subset of states plays the role of a subset of low-energy states close to the ground state of the system. We showed that by varying the system size, the bulk anisotropy and the boundary dissipative driving one can manipulate a number of peaks of the magnetization current, distance between the peaks in the parameter space, and their magnitudes. All the resulting stationary states are easily distinguishable by the value of the carried spin current, and by their nontrivial topology [35].

We expect the dissipative cooling approach considered in this paper to be effective also for other open quantum many body systems that are integrable via the off-diagonal Bethe ansatz method.

VP acknowledges financial support from the European Research Council through the advanced grant No. 694544—OMNES, and from the Deutsche Forschungsgemeinschaft through the DFG projects KL 645/20-1, KL 645/20-2. VP thanks the Department of Physics "E.R.Caianello" for hospitality and for short visits partial supports (FARB 2018 - 2019) during which the work was completed.

[1] F. Verstraete, M. M. Wolf, and J. I. Cirac, *NATURE PHYSICS* **5**, 633 (2009).
 [2] P. Zanardi and L. C. Venuti, *PHYSICAL REVIEW LETTERS* **113**, 10.1103/PhysRevLett.113.240406 (2014).
 [3] V. V. Albert, B. Bradlyn, M. Fraas, and L. Jiang, *PHYSICAL REVIEW X* **6**, 10.1103/PhysRevX.6.041031 (2016).
 [4] S. Touzard, A. Grimm, Z. Leghtas, S. O. Mundhada, P. Reinhold, C. Axline, M. Reagor, K. Chou, J. Blumoff, K. M. Sliwa, S. Shankar, L. Frunzio, R. J. Schoelkopf, M. Mirrahimi, and M. H. Devoret, *PHYSICAL REVIEW X* **8**, 10.1103/PhysRevX.8.021005 (2018).
 [5] D. C. Cole, J. J. Wu, S. D. Erickson, P.-Y. Hou, A. C. Wilson, D. Leibfried, and F. Reiter, *NEW JOURNAL OF PHYSICS* **23**, 10.1088/1367-2630/ac09c8 (2021).
 [6] A. P. Orioli, J. K. Thompson, and A. M. Rey, *PHYSICAL REVIEW X* **12**, 10.1103/PhysRevX.12.011054 (2022).
 [7] G. Barontini, L. Hohmann, F. Haas, J. Esteve, and J. Reichel, *SCIENCE* **349**, 1317 (2015).
 [8] T. Botzung, S. Diehl, and M. Müller, *Phys. Rev. B* **104**, 184422 (2021).
 [9] C.-E. Bardyn, M. A. Baranov, C. V. Kraus, E. Rico, A. Imamoglu, P. Zoller, and S. Diehl, *New Journal of Physics* **15**, 085001 (2013).

[10] C. Kollath, A. Sheikhan, S. Wolff, and F. Brennecke, *Phys. Rev. Lett.* **116**, 060401 (2016).
 [11] J. T. Barreiro, M. Mueller, P. Schindler, D. Nigg, T. Monz, M. Chwalla, M. Hennrich, C. F. Roos, P. Zoller, and R. Blatt, *NATURE* **470**, 486 (2011).
 [12] B. Kraus, H. P. Buechler, S. Diehl, A. Kantian, A. Micheli, and P. Zoller, *PHYSICAL REVIEW A* **78**, 10.1103/PhysRevA.78.042307 (2008).
 [13] N. Yamamoto, *Phys. Rev. A* **72**, 024104 (2005).
 [14] V. Popkov and G. M. Schütz, *PHYSICAL REVIEW E* **95**, 10.1103/PhysRevE.95.042128 (2017).
 [15] V. Popkov, X. Zhang, and A. Klümper, *Phys. Rev. B* **104**, L081410 (2021).
 [16] X. Zhang, A. Klümper, and V. Popkov, *Phys. Rev. B* **103**, 115435 (2021).
 [17] X. Zhang, A. Klümper, and V. Popkov, *Phys. Rev. B* **104**, 195409 (2021).
 [18] B. MISRA and E. SUDARSHAN, *JOURNAL OF MATHEMATICAL PHYSICS* **18**, 756 (1977).
 [19] K. Koshino and A. Shimizu, *PHYSICS REPORTS-REVIEW SECTION OF PHYSICS LETTERS* **412**, 191 (2005).
 [20] W. ITANO, D. HEINZEN, J. BOLLINGER, and D. WINELAND, *PHYSICAL REVIEW A* **41**, 2295 (1990).
 [21] P. Facchi, V. Gorini, G. Marmo, S. Pascazio, and E. S. Sudarshan, *PHYSICS LETTERS A* **275**, 12 (2000).
 [22] P. N. Jepsen, W. W. Ho, J. Amato-Grill, I. Dimitrova, E. Demler, and W. Ketterle, *Phys. Rev. X* **11**, 041054 (2021).
 [23] P. N. Jepsen, Y. K. E. Lee, H. Lin, I. Dimitrova, Y. Margalit, W. W. Ho, and W. Ketterle, *Nature Phys.* **18**, 899 (2022), arXiv:2110.12043 [cond-mat.quant-gas].
 [24] H. P. Breuer and F. Petruccione, *The theory of open quantum systems* (Oxford University Press, Great Clarendon Street, 2002).
 [25] See Supplemental Material.
 [26] H. SPOHN, *LETTERS IN MATHEMATICAL PHYSICS* **2**, 33 (1977).
 [27] V. Popkov, S. Essink, C. Presilla, and G. Schuetz, *PHYSICAL REVIEW A* **98**, 10.1103/PhysRevA.98.052110 (2018).
 [28] Phantom Bethe roots criterium for open XXZ spin chain with boundary fields is given by Eq.(17) of [16]. For our special case h_D (1) we set $\alpha_+ = \alpha_- = -\eta = -i\gamma$, $\beta_+ + \beta_- = 0$, $\theta_- = i(\pi - \varphi_L)$, $\theta_+ = i(\pi - \varphi_R)$, $1/\cosh(\beta_-) = \sin\theta_L$, $\tanh(\beta_-) = -\cos\theta_L$, leading to Eq.(8), with $M = 0, \dots, N - 1$. Another choice of parameters $\alpha_+ = \alpha_- = \eta = i\gamma$, $\beta_+ + \beta_- = 0$, $\theta_- = -i\varphi_L$, $\theta_+ = -i\varphi_R$, $1/\cosh(\beta_-) = \sin\theta_L$, $\tanh(\beta_-) = \cos\theta_L$ leads to the same h_D . Inserting it into Eq.(17) of [16] leads to the same Eq.(8) with $M \rightarrow M + 2$, thus enlarging the M range in (8) to values $M = 0, \dots, N + 1$.
 [29] V. Popkov, S. Essink, C. Kollath, and C. Presilla, *Phys. Rev. A* **102**, 032205 (2020).
 [30] V. Popkov, C. Presilla, and J. Schmidt, *PHYSICAL REVIEW A* **95**, 10.1103/PhysRevA.95.052131 (2017).
 [31] V. Popkov, J. Schmidt, and C. Presilla, *JOURNAL OF PHYSICS A-MATHEMATICAL AND THEORETICAL* **50**, 10.1088/1751-8121/aa86cb (2017).
 [32] M. Salerno and V. Popkov, *Phys. Rev. E* **87**, 022108 (2013).
 [33] V. Popkov, T. Prosen, and L. Zadnik, *PHYSICAL REVIEW LETTERS* **124**, 10.1103/Phys-

- [RevLett.124.160403](#) (2020).
- [34] V. Popkov, X. Zhang, and T. Prosen, Boundary driven XYZ chain: Exact inhomogeneous triangular matrix product ansatz, [arXiv:arXiv:2112.05616](#) [cond-mat.stat-mech].
- [35] T. Posske and M. Thorwart, *Phys. Rev. Lett.* **122**, 097204 (2019).
- [36] V. Popkov, T. Prosen, and L. Zadnik, *PHYSICAL REVIEW E* **101**, [10.1103/PhysRevE.101.042122](#) (2020).

Supplemental Material for
**Dissipative cooling towards phantom Bethe states
in boundary driven XXZ spin chain**

by Vladislav Popkov and Mario Salerno

This Supplemental Material contains four sections organized as follows. In **S-I** we collect some useful standard definitions. In **S-II** we derive symmetry properties of the Lindblad equation. In **S-III** we prove the existence of invariant subspaces at Bethe manifolds (8). In **S-IV** we analyze the effective Markov process (3).

S-I. LINDBLAD MASTER EQUATION AND SYSTEM EVOLUTION NEAR ZENO LIMIT

A density matrix of a generic quantum system with dissipation satisfies, under standard assumptions [18, 24], a Lindblad Master equation (LME),

$$\begin{aligned} \frac{\partial \rho(t)}{\partial t} &= -i[H_s, \rho] + \Gamma \mathcal{D}[\rho] \\ \mathcal{D}[\rho] &= \sum_{\gamma} \mathcal{D}_{L_{\gamma}}[\rho] = \sum_{\gamma} 2L_{\gamma} \rho L_{\gamma}^{\dagger} - (L_{\gamma}^{\dagger} L_{\gamma} \rho + \rho L_{\gamma}^{\dagger} L_{\gamma}), \end{aligned} \quad (\text{S1})$$

where $H_s^{\dagger} = H_s$ is a coherent part, $\mathcal{D}[\rho]$ is the dissipator, and L_{γ} are Lindblad operators, describing the interaction with the environment. In our model H_s is taken as the Heisenberg XXZ Hamiltonian with z anisotropy $J_z/J_x = J_z/J_y = \Delta$:

$$H_s = \sum_{n=0}^N \sigma_n^x \sigma_{n+1}^x + \sigma_n^y \sigma_{n+1}^y + \Delta \sigma_n^z \sigma_{n+1}^z = \sum_{n=0}^N \vec{\sigma}_n \cdot \hat{J} \vec{\sigma}_{n+1}, \quad (\text{S2})$$

with $\hat{J} = \text{diag}(1, 1, \Delta)$. The chain consists of $N + 2$ sites, numbered as $0, 1, \dots, N + 1$, and is coupled at the edges, i.e. at sites 0 and $N+1$, to magnetic reservoirs modeled by Lindblad operators, L_i , $i = L, R$ for left edge ($L \equiv \text{site } 0$) and right edge ($R \equiv \text{site } N + 1$), respectively, constraining boundary spins to relax to generic pure qubit states of the form

$$\rho_{L,R} = \frac{1}{2} (I + \vec{n}_{L,R} \cdot \vec{\sigma}), \quad (\text{S3})$$

with \vec{n}_L, \vec{n}_R unit vectors of polarization, parametrized by spherical coordinates angles $0 \leq \theta_L, \theta_R \leq \pi$ and $0 \leq \varphi_L, \varphi_R < 2\pi$.

The explicit form of $L_{L,R}$ can be obtained by observing that the targeting of a pure qubit state $|\psi\rangle\langle\psi|$ at a single site, is achieved by means of operators L of the form $L = |\psi\rangle\langle\psi^{\perp}|$, with $\langle\psi^{\perp}|\psi\rangle = 0$, so that the dissipator $\mathcal{D}_L[\rho]$ automatically satisfies $\mathcal{D}_L[|\psi\rangle\langle\psi|] = 0$. Observing that the normalization of the states $|\psi\rangle, |\psi^{\perp}\rangle$ entails $\text{tr}(L^{\dagger}L) = 1$ and that the linear map $\mathcal{D}_L[\rho]$ has four eigenmodes with eigenvalues $0, -1, -1, -2$, one can write a formal solution, valid for large times t , of the Eq. (S1) with $H_s \rightarrow 0$ and with a single operator $L = |\psi\rangle\langle\psi^{\perp}|$, as:

$$\rho_1(t) = e^{-\Gamma \mathcal{D}_L t} \rho_1(0) = |\psi\rangle\langle\psi| + O(e^{-\Gamma t}). \quad (\text{S4})$$

Note that a similar solution can be written also for $\Gamma \gg \|H_s\|$, i.e. when the coherent evolution can be considered as a small perturbation. From the above it follows that the targeting of the pure states at the edges

$$\begin{aligned} \rho_{L,R} &= |\psi_{L,R}\rangle\langle\psi_{L,R}| \\ \langle\psi_{\gamma}| &= \left(\cos \frac{\theta_{\gamma}}{2}, \quad e^{-i\varphi_{\gamma}} \sin \frac{\theta_{\gamma}}{2} \right), \quad \gamma = L, R, \end{aligned}$$

can be achieved by a dissipator \mathcal{D} in (S1) with Lindblad operators

$$L_1 = |\psi_L\rangle\langle\psi_L^{\perp}| \otimes I^{\otimes N+1}, \quad (\text{S5})$$

$$L_2 = I^{\otimes N+1} \otimes |\psi_R\rangle\langle\psi_R^{\perp}|, \quad (\text{S6})$$

acting at sites 0, $N + 1$, respectively. It can be proved that the steady state, $\rho_{NESS}(\Gamma) = \lim_{t \rightarrow \infty} \rho(\Gamma, t)$, of (S1) is unique for any given choice of the targeted polarizations and in the Zeno limit we have

$$\lim_{\Gamma \rightarrow \infty} \rho_{NESS}(\Gamma) = \rho_{NESS}^{Zeno} = \rho_L \otimes R \otimes \rho_R. \quad (\text{S7})$$

We also recall (see [27] for details) that at time scale $t = O(1)$ and large Γ , the density matrix $\rho(t)$ acquires the approximate form (S7) with $R \equiv R(t\Gamma) = R(\tau)$, evolving in time according to

$$\frac{\partial R(\tau)}{\partial \tau} = -i[h_D, R] + \frac{1}{\Gamma} \mathcal{D}_{eff}[R] \quad (\text{S8})$$

where $\mathcal{D}_{\{\}}^{\dagger}$ is an effective dissipator and $h_D = h_D^{\dagger}$ is the so-called dissipation-projected Hamiltonian [2] given in Eq.(1) of the main text. From Eqs. (S7), (S8) it follows that $[h_D, R] = 0$ and R is given by

$$R(\tau) = \sum_{\alpha} P_{\alpha}(\tau) |\alpha\rangle \langle \alpha| + O(\Gamma^{-1}), \quad (\text{S9})$$

with $|\alpha\rangle$ denoting h_D eigenvectors. Moreover, the coefficients $P_{\alpha}(\tau)$ evolve adiabatically under the perturbative effective dissipator \mathcal{D}_{eff} in (S8). The adiabatic evolution is given by the Markov process discussed in sec. S-IV. Remarkably, it was shown in [36] that the Zeno NESS (S7) is robust against possible asymmetries of the dissipation between left and right boundaries, i.e. the asymmetric rescaling of the Lindblad operators $L_1 \rightarrow \delta_1 L_1, L_2 \rightarrow \delta_2 L_2$ in (S1), with any finite nonzero δ_1, δ_2 values, yields the same limiting result (S7).

S-II. SYMMETRY PROPERTIES OF THE LINDBLAD EQUATION

In the following we investigate symmetry properties of the NESS of the Lindblad equation (S1) with targeted polarizations lying in XY -plane, $\theta_L = \theta_R = \pi/2$, $\varphi_L = 0$, and arbitrary φ_R . For this we introduce the operator U_{φ} performing a simultaneous rotation of all spins around the z axis and the parity operator \mathcal{P} , respectively defined as

$$U_{\varphi} = \prod_{k=0}^{N+1} e^{i\frac{\varphi}{2}\sigma_k^z}, \quad \mathcal{P} := S_n \rightarrow S_{N-n+1}, \quad n = 0, 1, \dots, N+1.$$

Notice that the bulk Hamiltonian H_s commute with both operators U_{φ} and \mathcal{P} and hence also with their product $U_{\varphi}\mathcal{P} \equiv \mathcal{U}_{\varphi}$, i.e. $[H, \mathcal{U}_{\varphi}] = 0$. On the other hand the Lindblad operators L_1, L_2 from (S5), (S6), under the action of \mathcal{U}_{φ_R} transform as:

$$\begin{aligned} \mathcal{U}_{\varphi_R} L_2 \mathcal{U}_{\varphi_R}^{\dagger} &= L_1, \\ \mathcal{U}_{\varphi_R} L_1 \mathcal{U}_{\varphi_R}^{\dagger} &= e^{i\varphi_R \sigma_{N+1}^z} L_2 e^{-i\varphi_R \sigma_{N+1}^z} = L_2|_{\varphi_R \rightarrow -\varphi_R}, \end{aligned}$$

i.e. one gets the same physical setup but with the opposite boundary gradient at the right boundary. Indeed, it is straightforward to verify that LME (S1) under the \mathcal{U} transformation is mapped onto the same LME but with opposite boundary gradient, $\varphi_R \rightarrow -\varphi_R$, with the corresponding ρ matrix transformed as

$$\rho(-\varphi_R) = \mathcal{U}_{\varphi_R} \rho(\varphi_R) \mathcal{U}_{\varphi_R}^{\dagger}. \quad (\text{S10})$$

The uniqueness of the NESS for any choice of the boundary parameters, implies that the above transformation is a map between NESS of opposite boundary gradients. On the other hand, taking into account that $M_+ + M_- = N + 1$ we have, from the φ_R angles parametrized by the integer M_+ in Eq.(8), that:

$$\varphi_R(M_-) \equiv (N + 1 - 2M_-)\gamma = (N + 1 - 2(N + 1 - M_+))\gamma = -(N + 1 - 2M_+)\gamma = -\varphi_R(M_+), \quad (\text{S11})$$

thus the transformation (S10) allows to get the M_- -NESS from the M_+ one as:

$$\rho_{NESS}(\varphi_R(M_-)) = \mathcal{U}_{\varphi_R(M_+)} \rho_{NESS}(\varphi_R(M_+)) \mathcal{U}_{\varphi_R(M_+)}^{\dagger}. \quad (\text{S12})$$

Notably, the steady state current under the transformation $\varphi_R \rightarrow -\varphi_R$ changes its sign: $\langle j^z(M_-) \rangle = -\langle j^z(M_+) \rangle$, in agreement with what observed in Fig. 2 and Fig. 3 of the main text.

S-III. INVARIANT SUBSPACE W_M OF h_D AT PHANTOM BETHE MANIFOLDS

To investigate the invariant phantom Bethe manifolds it is convenient to introduce the following parametrization for an arbitrary pure qubit state

$$|f, F\rangle = \frac{1}{\sqrt{1 + e^{2f}}} \begin{pmatrix} 1 \\ e^{f+iF} \end{pmatrix}, \quad (\text{S13})$$

$$|F\rangle = \frac{1}{\sqrt{2}} \begin{pmatrix} 1 \\ e^{iF} \end{pmatrix}, \quad (\text{S14})$$

where f, F are real numbers. Notice that the state $|f, F\rangle$ describes a spin 1/2 pointing in the direction $(\langle\sigma^x\rangle, \langle\sigma^y\rangle, \langle\sigma^z\rangle) = (\sin\theta \cos F, \sin\theta \sin F, \cos\theta)$ with $\tan(\theta/2) = e^f$, thus $-\infty < f < \infty$, parametrizes the polar angle while $0 \leq F < 2\pi$ parametrizes the azimuthal angle (or phase factor) of the usual polar coordinate system. The state $|F\rangle$ instead, describes a fully polarized spin 1/2 lying in XY -plane. Here for simplicity we consider the condition (8) at $\theta = \pi/2$ (dissipation baths polarizations in the XY plane) to prove the following Theorem.

Theorem The set of states

$$|n_1, n_2, \dots, n_M\rangle = \bigotimes_{k=1}^{n_1-1} |k\varphi\rangle \bigotimes_{k=n_1}^{n_2-1} |(k-2)\varphi\rangle \dots \bigotimes_{k=n_M}^N |(k-2M)\varphi\rangle, \quad (\text{S15})$$

$$1 \leq n_1 < n_2 < \dots < n_M \leq N + 1, \quad (\text{S16})$$

form an invariant subspace W_M^+ of h_D (1) satisfying Eq. (8) with fixed M and $\varphi_L = 0$.

Remark.— In (S15) $n_1 = 1$ and $n_M = N + 1$ denote virtual kinks at outer links of the chain $(0, 1)$ and $(N, N + 1)$: $n_1 = 1$ and $n_1 > 1$ correspond to first qubit in (S15) being $|-\varphi\rangle$ and $|\varphi\rangle$ respectively. Likewise, $n_M = N + 1$ and $n_M < N + 1$ correspond to the last qubit of the form $|(N - 2M + 2)\varphi\rangle$ and $|(N - 2M)\varphi\rangle$ respectively. Introducing the notation

$$|F_1, F_2, \dots, F_m\rangle = 2^{-m/2} \bigotimes_{k=1}^m \begin{pmatrix} 1 \\ e^{iF_k} \end{pmatrix}, \quad (\text{S17})$$

$$F^\perp = F + \pi; \quad |F^\perp\rangle = \sigma^z |F\rangle; \quad \langle F^\perp | F \rangle = 0, \quad (\text{S18})$$

the operator $\tilde{h}_D = h_D - (N - 1)\Delta I$ can be written as sum of local terms

$$\tilde{h}_D = h_{12} + h_{23} + \dots + h_{N-1, N} + h_l \otimes I^{\otimes N-1} + I^{\otimes N-1} \otimes h_r, \quad (\text{S19})$$

where $h = \sigma^x \otimes \sigma^x + \sigma^y \otimes \sigma^y + \Delta(\sigma^z \otimes \sigma^z - I \otimes I)$ is the local energy-density of the XXZ spin chain.

A key point in the proof is the divergence condition:

$$h|F, F + \gamma\rangle = -\kappa|F^\perp, F + \gamma\rangle + \kappa|F, (F + \gamma)^\perp\rangle, \quad (\text{S20})$$

$$\kappa = i \sin \gamma,$$

$$\Delta = \cos \gamma. \quad (\text{S21})$$

Using (S20) one obtains the following useful relations:

$$(h_{12} + h_{23})|F, F + \gamma, F\rangle = -\kappa|F^\perp, F + \gamma, F\rangle - \kappa|F, F + \gamma, F^\perp\rangle + a_0|F, F + \gamma, F\rangle + a_+|F, F - \gamma, F\rangle, \quad (\text{S22})$$

$$(h_{12} + h_{23})|F, F - \gamma, F\rangle = \kappa|F^\perp, F - \gamma, F\rangle + \kappa|F, F - \gamma, F^\perp\rangle + a_0|F, F - \gamma, F\rangle + a_-|F, F + \gamma, F\rangle, \quad (\text{S23})$$

$$a_0 = -2\Delta, \quad a_\pm = 2e^{\pm i\gamma}. \quad (\text{S24})$$

Due to (S20), (S22), (S23), any factorized state of the form:

$$\Psi = \bigotimes_{k=1}^N |0, F_k\rangle, \quad \text{with} \quad F_{k+1} - F_k = \pm\gamma, \quad (\text{S25})$$

under the action of the operator $\sum_{n=1}^{N-1} h_{n, n+1}$ will transform into a sum of terms Ψ_α of the same type of (S25), i.e. $\Psi_\alpha = \bigotimes_{k=1}^N |F_{k, \alpha}\rangle$, with $F_{k+1, \alpha} - F_{k, \alpha} = \pm\gamma$, plus two extra terms :

$$\sum_{n=1}^{N-1} h_{n, n+1} \Psi = \sum_{\alpha} C_\alpha |F_1, F_{2, \alpha}, F_{3, \alpha}, \dots, F_{N-1, \alpha}, F_N\rangle + A_1 |F_1^\perp, F_2, \dots, F_N\rangle + A_N |F_1, F_2, \dots, F_{N-1}, F_N^\perp\rangle,$$

$$F_{2\alpha} - F_1 = \pm\gamma, \quad F_{(k+1), \alpha} - F_{k, \alpha} = \pm\gamma; \quad F_N - F_{N-1, \alpha} = \pm\gamma,$$

with $A_1 = \kappa \text{sign}((F_1 - F_2)/\gamma)$ and $A_N = \kappa \text{sign}((F_N - F_{N-1})/\gamma)$. All basis vector of W_M are of the form (S17) with $F_1 = \pm\gamma$, $F_N = F_c(M) \pm \gamma$. By acting with \tilde{h}_D on the basis elements $\|n_1 n_2 \dots n_M\rangle\rangle$, we generate other terms of the same basis $\|m_1 m_2 \dots m_M\rangle\rangle \equiv |F_1, \dots, F_N\rangle$ and extra terms with "impurities" at site 1 and site N :

$$\begin{aligned} \tilde{h}_D \|n_1 n_2 \dots n_M\rangle\rangle &= \dots + A_1 |F_1^\perp, F_2, \dots\rangle + h_l \otimes I^{\otimes N-1} |F_1^\perp, F_2, \dots\rangle + \\ &+ A_N |\dots F_{N-1}, F_N^\perp\rangle + (I^{\otimes N-1} \otimes h_r) |\dots, F_{N-1}, F_N^\perp\rangle. \end{aligned}$$

Since $A_1 = \text{sign}((F_1 - F_2)/\gamma)\kappa$ and $F_1 = \pm\gamma$, we have that the following four $A_1 |F_1^\perp, F_2 \dots\rangle$ terms may arise:

$$A_1 |F_1^\perp, F_2, \dots\rangle = \kappa |-\gamma^\perp, -2\gamma, \dots\rangle, \quad -\kappa |\gamma^\perp, 2\gamma, \dots\rangle, \quad (\text{S26})$$

$$A_1 |F_1^\perp, F_2, \dots\rangle = \kappa |\gamma^\perp, 0, \dots\rangle, \quad -\kappa |-\gamma^\perp, 0, \dots\rangle. \quad (\text{S27})$$

Terms of type (S26) cancel with respective terms from $h_l \otimes I^{\otimes N-1} |F_1, F_2 \dots\rangle$, using the relations

$$h_l |\pm\gamma\rangle = \pm\kappa |\pm\gamma^\perp\rangle + \Delta |\pm\gamma\rangle, \quad (\text{S28})$$

and similarly, one get cancelation of the terms of type (S27) by means of the relations

$$h_l |\pm\gamma\rangle = \mp\kappa |\pm\gamma^\perp\rangle - \Delta |\pm\gamma\rangle + 2e^{\pm i\gamma} |\mp\gamma\rangle. \quad (\text{S29})$$

Proceedings in the same manner for the arising four terms of type $A_N |\dots F_{N-1}, F_N^\perp\rangle$:

$$A_N |\dots F_{N-1}, F_N^\perp\rangle = -\kappa |\dots, \Phi_c + 2\gamma, (\Phi_c + \gamma)^\perp\rangle, \quad \kappa |\dots, \Phi_c - 2\gamma, (\Phi_c - \gamma)^\perp\rangle, \quad (\text{S30})$$

$$A_N |\dots F_{N-1}, F_N^\perp\rangle = \kappa |\dots, \Phi_c, (\Phi_c + \gamma)^\perp\rangle, \quad -\kappa |\dots, \Phi_c, (\Phi_c - \gamma)^\perp\rangle, \quad (\text{S31})$$

with

$$\Phi_c(M) = (N + 1 - 2M)\gamma, \quad (\text{S32})$$

one finds that terms (S30),(S31) cancel with respective terms $I^{\otimes N-1} \otimes h_r |\dots F_{N-1}, F_N\rangle$ using relations

$$h_r |\Phi_c \pm \gamma\rangle = \pm\kappa |(\Phi_c \pm \gamma)^\perp\rangle + \Delta |\Phi_c \pm \gamma\rangle, \quad (\text{S33})$$

$$h_r |\Phi_c \pm \gamma\rangle = \mp\kappa |(\Phi_c \pm \gamma)^\perp\rangle - \Delta |\Phi_c \pm \gamma\rangle + 2e^{\pm i\gamma} |\Phi_c \mp \gamma\rangle, \quad (\text{S34})$$

respectively (note that relations (S33), (S34) differ from (S28), (S29) simply by the increase of the angle by $\Phi_c(M)$). From this we conclude that the action of h_D on any basis vector of W_M produces states that still belong to W_M , thus proving the Theorem (QED). We close this section with the following remarks.

Remark 1.– It can be shown that the repeated action of h_D on any single basis vector generates the whole subspace W_M . Moreover, it follows that all eigenvectors $|\alpha_+\rangle \in W_M$ of h_D have nonzero overlaps with all vectors $\|n_1 \dots n_M\rangle\rangle$ of W_M basis. The total number of states in W_M in (S15) can be calculated combinatorially as:

$$\dim W(M) = \binom{N+1}{M} = \binom{N}{M} + \binom{N}{M-1}.$$

Remark 2.– The subspace W_M is a part of a larger invariant subspace G_M^+ described in [16]. G_M^+ contains all vectors of W_M plus additional linearly independent vectors, all with qualitatively the same chirality features. The total number of vectors in G_M^+ is

$$\dim G_M^+ = \binom{N}{M} + \binom{N}{M-1} + \binom{N}{M-2} + \dots + \binom{N}{0},$$

see [16]. The appearance of smaller invariant subspace $W(M)$ within G_M^+ is a consequence of a special form of the boundary fields in the dissipation-projected Hamiltonian (1).

S-IV. PROPERTIES OF MARKOV PROCESS (3) AT POINTS $\Phi_c(M)$

The effective Markov evolution for the probabilities P_α of the occupation of state α at time τ :

$$\frac{\partial P_\alpha(\tau)}{\partial \tau} = \sum_{\beta \neq \alpha} w_{\beta\alpha} P_\beta(\tau) - \sum_{\beta \neq \alpha} w_{\alpha\beta} P_\alpha(\tau) \quad (\text{S35})$$

is related to a reduced density matrix dynamics $R(\tau)$, near the quantum Zeno limit, given by

$$R(\tau) \approx \sum_{\alpha=1}^{\dim \mathcal{H}} P_\alpha(\tau) |\alpha\rangle \langle \alpha|,$$

where $\dim \mathcal{H} = 2^N$ is the dimension of the Hilbert space, and $|\alpha\rangle$ are eigenvectors of h_D . The rates $w_{\alpha\beta} \equiv w_{\alpha \rightarrow \beta}$ are given by [27]:

$$w_{\alpha\beta} = |\langle \beta | g_L | \alpha \rangle|^2 + |\langle \beta | g_R | \alpha \rangle|^2, \quad (\text{S36})$$

where g_L, g_R are some locally acting operators[27]. On phantom Bethe manifolds parametrized by the integer number M , the existence of invariant subspaces of h_D : G_M^+, G_M^- and $W_M \in G_M^+$ allows to split the h_D eigenvectors $|\alpha\rangle$ into three blocks, as

$$\begin{aligned} R(t) \approx & \sum_{\alpha_+^{(1)}=1}^{\dim(W_M)} P(\alpha_+^{(1)}, t) |\alpha_+^{(1)}\rangle \langle \alpha_+^{(1)}| + \\ & + \sum_{\alpha_+^{(2)}=1}^{\dim(G_M^+) - \dim(W_M)} P(\alpha_+^{(2)}, t) |\alpha_+^{(2)}\rangle \langle \alpha_+^{(2)}| + \\ & + \sum_{\alpha_-=1}^{\dim(G_M^-)} P(\alpha_-, t) |\alpha_-\rangle \langle \alpha_-\rangle, \end{aligned} \quad (\text{S37})$$

corresponding to respective h_D eigenvalues $\{\lambda_{\alpha_+^{(1)}}\}$, $\{\lambda_{\alpha_+^{(2)}}\}$ and $\{\lambda_{\alpha_-}\}$. In the Eq (S37), the first two block contributions share the same chirality (indicated with " + " subscript). It was proved in [16] that states in G_M^+, G_M^- are mutually orthogonal. If the sets $\{\lambda_{\alpha_+^{(1)}}\}$, $\{\lambda_{\alpha_+^{(2)}}\}$ have no intersection,

$$\{\lambda_{\alpha_+^{(1)}}\} \cap \{\lambda_{\alpha_+^{(2)}}\} = \emptyset, \quad (\text{S38})$$

then also states $|\alpha_+^{(1)}\rangle$, $|\alpha_+^{(2)}\rangle$ are also orthogonal.

We will be interested in cumulative probability current towards set of states in W_M from other blocks, given by

$$J_{\alpha_-, \alpha_+^{(2)} \rightarrow \alpha_+^{(1)}}(t) = \sum_{\alpha_+^{(1)}: |\alpha_+^{(1)}\rangle \in W_M} \sum_{\beta: |\beta\rangle \notin W_M} \left(P(\beta, t) w_{\beta\alpha_+^{(1)}} - P(\alpha_+^{(1)}, t) w_{\alpha_+^{(1)}\beta} \right) \quad (\text{S39})$$

First, notice that all basis vectors $||n_1, n_2, \dots, n_M\rangle\rangle$ of W_M are eigenvectors of operators g_L, g_R in (S36):

$$\begin{aligned} g_L ||n_1, n_2, \dots, n_M\rangle\rangle &= (2\delta_{n_1,1} - 1) i \sin \varphi ||n_1, n_2, \dots, n_M\rangle\rangle, \\ g_R ||n_1, n_2, \dots, n_M\rangle\rangle &= (1 - 2\delta_{n_M, N+1}) i \sin \varphi ||n_1, n_2, \dots, n_M\rangle\rangle, \end{aligned}$$

entailing all

$$w_{\alpha_+^{(1)}\beta} = 0; \quad |\alpha_+^{(1)}\rangle \in W_M, \quad |\beta\rangle \notin W_M, \quad (\text{S40})$$

provided (S38). On the other hand, at least some of the $w_{\beta\alpha_+^{(1)}}$ rates in (S39) are strictly positive, since W_M basis states $\langle\langle n_1 n_2 \dots n_M |$ are not left eigenvectors of g_L, g_R . Consequently,

$$w_{\beta\alpha_+^{(1)}} > 0; \quad |\alpha_+^{(1)}\rangle \in W_M, \quad |\beta\rangle \notin W_M, \text{ for some } \beta. \quad (\text{S41})$$

Eqs(S40), (S41) show that one has strictly positive probability current (S39) at all times, leading to gradual increase of cumulative population of states with the same chirality $\sum P(\alpha_+^{(1)}, t)$ with time, and depopulation of all other states. In the long time limit, only contributions from the invariant subspace W_M in (S37) remain, leading to

$$R(t \rightarrow \infty) = \sum_{\alpha_+^{(1)}=1}^{\dim(W_M)} P(\alpha_+^{(1)}) |\alpha_+^{(1)}\rangle \langle \alpha_+^{(1)}| + O(\Gamma^{-1}).$$